Interpretation of low-energy electron-CO_2 scattering

W. Vanroose,[1,*] C. W. McCurdy,[1,2,†] and T. N. Rescigno[1,3,‡]
[1]*Lawrence Berkeley National Laboratory, Computing Sciences, Berkeley, California 94720*
[2]*Department of Applied Science, University of California-Davis, Livermore, California 94551*
[3]*Lawrence Livermore National Laboratory, Physics and Advanced Technologies, Livermore, California 94551*
(Received 1 April 2002; published 27 September 2002)

Recent *ab initio* calculations of low-energy electron-CO_2 scattering [Rescigno *et al.*, Phys. Rev. A **65**, 032716 (2002)] are interpreted using an analytically solvable model. The model, which treats two partial-wave Hamiltonians with different l values coupled by a long-range (d/r^2) interaction, is a generalization of similar single-channel models that have previously been used to interpret the low-energy behavior of electron scattering by polar diatomic molecules. The present model is used to track the pole trajectories of both resonances and virtual states, both of which figure prominently in low-energy electron-CO_2 scattering, in the plane of complex momentum. The connection between resonant and virtual states is found to display a different topology in the case of a polyatomic molecule than it does in diatomic molecules. In a polyatomic molecule, these states may have a conical intersection and consequently acquire a Berry phase along closed paths in two-dimensional vibrational motion. The analytic behavior of the S matrix is further modified by the presence of a geometry-dependent dipole moment.

DOI: 10.1103/PhysRevA.66.032720 PACS number(s): 34.80.Gs, 03.65.Nk

I. INTRODUCTION

There has been considerable activity over the past few years, both theoretical and experimental, on the subject of low-energy electron-CO_2 collisions. The principal features of the low-energy cross sections, namely the dramatic rise in the total cross section below 2 eV and the resonance feature near 3.8 eV, have been known for many years and have been the subject of many theoretical investigations. However, the ability of first-principles theory to quantitatively reproduce and explain features of the observed cross sections at low energy is a relatively recent development. For example, it was not until 1998 that an *ab initio* study was performed which was able to conclusively show that the low-energy rise in the elastic cross was the result of a virtual state [1], although this fact had been suggested by earlier model studies [2]. Only recently has *ab initio* theory correctly accounted for both the low-energy behavior and the resonance peak [3,4] or been able to achieve quantitatively correct differential cross sections below 6 eV [3].

There have also been advances on the experimental front. Low-energy electron beams produced by atomic photoionization have been used to perform scattering experiments down to 10 meV, giving clear experimental evidence for the CO_2^- virtual state [5]. The unprecedented energy resolution (7 meV) recently achieved by Allan [6] with electron spectrometers allowed him to resolve electron energy-loss peaks for nearly degenerate vibrational levels in CO_2 and to make separate measurements of the excitation cross sections for each member of the lowest Fermi dyad with high accuracy. The essential features of these resonant vibrational excitation cross sections were accurately reproduced in the most recent work of Rescigno *et al.* [7], who extended their earlier fixed-nuclei calculations [3] to include the effects of both symmetric stretch and bending and carried out a multidimensional treatment of the nuclear dynamics on a complex local resonance surface constructed from the fixed-nuclei results. Nevertheless, there are features of the measured cross sections, such as subtle interference structures in the resonant cross sections and the strikingly different behavior of the excitation functions for the individual Fermi levels on the low energy side of the resonance region, that raise additional questions and leave ample room for future theoretical work. There are also interesting questions that arise from an examination of the *ab initio* results which would be difficult to address with large-scale first-principles calculations. For this reason, we present calculations here on several model problems whose analytic structure can be examined in detail and which are expected to reflect key aspects of the true physical problem. The purpose of this exercise is to gain a deeper insight into the nuclear dynamics of electron-CO_2 scattering which will hopefully suggest possible directions for further *ab initio* work.

It is well known that the CO_2 molecule, in its equilibrium geometry, *cannot* bind an additional electron to form a stable negative ion. We find instead a virtual state of $^2\Sigma_g^+$ symmetry and a $^2\Pi_u$ resonance state. It is also well known [8,9] that CO_2^- becomes electronically bound, in $^2A_1$ symmetry, if the molecule is either stretched or bent sufficiently. An examination of the fixed-nuclei resonance parameters for the $^2\Pi_u$ negative ion state shows that as the molecule is stretched, in linear geometry, the resonance width decreases monotonically as its energy, relative to neutral CO_2, approaches zero, i.e., the resonance evolves smoothly to become a bound state. Once bound, we can further track the ion energy, defined now as the lowest eigenvalue of the fixed-nuclei Hamiltonian for the anion, to its minumum by bending the molecule. So we would say that the $^2A_1$ anion correlates with the $^2\Pi_u$ shape resonance.

*Electronic address: wivanroose@lbl.gov
†Electronic address: cwmccurdy@lbl.gov
‡Electronic address: tnr@llnl.gov

But what if we start by bending the molecule first? The fixed-nuclei calculations show that the resonance rapidly broadens as the molecule is bent; the practical consequence of this behavior is that the resonance gets washed out and has no visible effect on the fixed-nuclei cross section for angles greater than about 15°. However, for sufficiently large angles (greater than 30°) the fixed-nuclei Hamiltonion again shows a stable negative ion. Does the ion again connect smoothly to the resonance or is it perhaps the $^2\Sigma_g^+$ virtual state that correlates with the bound negative ion? And how can the correlation diagram depend on the path one takes from the initial linear geometry to the final geometry that characterizes the bound negative ion? Our earlier *ab initio* study [7] could not address this question. The dynamics in those calculations are completely insensitive to the topology of the resonance surface where the width is large, since the wave packet rapidly decays in such regions.

For this reason, we investigate here a model problem in which the interaction between a resonance and a virtual state can be examined in detail. We will see that the nature of the coupling that produces an interaction between the two states has a profound effect on the pole trajectories. We contrast the behavior one finds when the coupling is of short-range with the case of long-range dipole coupling that more accurately reflects the situation that pertains to bent CO_2^-. We emphasize that it is not our intention here to present a model with parameters that are tuned to reproduce either our earlier *ab initio* [3,7] or measured cross sections. Indeed, the behavior of the electron-CO_2 cross sections below 1 eV collision energy has been quantitatively reproduced in earlier model studies [10–12]. Our purpose here is to focus on the topology of the electronic surfaces that produce the essential features in the observed cross sections, to point out the significant modifications (and to clarify some confusing points in the literature) caused by a geometry-dependent electron-dipole interaction, and to suggest a connection between the virtual state and the resonance state that has not previously been proposed. These considerations may be relevant in other collision systems and thus have implications that go beyond the issue of electron collisions with CO_2.

The outline of this paper is as follows. We begin in Sec. II with some remarks about a previously studied model—a square well plus a cutoff dipole potential—that has often been used to explain the physics of electron scattering by polar molecules [13–15]. We review some important differences between the analytic structure of that problem and the case of a short-range potential. In Sec. III we introduce an analytically solvable two-channel generalization of the model, motivated by a consideration of a single-center expansion of the physical wave function. In Secs. IV and V, respectively, we examine the behavior of the poles of the S matrix that is seen with either short-ranged or dipole coupling between the channels. In Sec. VI we discuss the case of a degeneracy in the virtual state and resonance trajectories which can produce a Berry phase in the resonance wave function. We conclude with a brief discussion. We employ atomic units throughout the paper.

II. POTENTIAL SCATTERING

Our objective is to study how the resonance states of a molecule with more than one nuclear degree of freedom become bound as the nuclear geometry is varied. Before tackling that problem, we first consider the simpler question of tracking the movement of a resonance state, defined here as a pole of the S matrix, in a single-channel radial scattering problem when some potential parameter is varied. The wave function is a solution of the Schrödinger equation $[H(r) - k^2/2]\psi(k,r)=0$ with the Hamiltonian defined as

$$H=-\frac{1}{2}d^2/dr^2+V(r), \tag{1}$$

$$V(r)=\begin{cases}\lambda V_0(r), & r<r_0\\ \dfrac{l(l+1)}{2r^2}, & r\geqslant r_0, \quad l \text{ integer},\end{cases} \tag{2}$$

where $V_0(r)$ is an attractive short-ranged potential. Note that the centrifugal term in Eq. (2) has been truncated at r_0 to avoid an unphysical singularity at $r=0$ in the case of noninteger l values which we allow later in this discussion. The truncation of the centrifugal potential in the interior of the interaction does not affect the qualitative behavior of the poles of the S matrix, which are solely determined by the asymptotic behavior of the effective potential. With these definitions, $S(k)$ is defined by the asymptotic behavior of the scattering wave function with respect to s-wave Ricatti-Hankel functions:

$$\psi(k,r) \underset{r\to\infty}{\sim} e^{-ikr}-S(k)e^{ikr}. \tag{3}$$

The behavior of the poles of $S(k)$ for such a problem is well known and is illustrated in Fig. 1. Suppose that the initial value of λ is chosen so that there is a resonance, defined as a pole of $S(k)$ in the lower half k plane. The symmetry requirement

$$S(-k^*)=S(k)^* \tag{4}$$

implies that, for $\mathrm{Re}(k)>0$, the poles must occur in pairs, symmetrically placed with respect to the imaginary k axis. If the potential well is deepened by increasing λ, the poles move toward the negative imaginary k axis and eventually collide, forming a double pole. The point of intersection is determined by the value of l. For $l=0$, the poles collide on the negative imaginary axis; as λ is further increased, one pole moves up the axis, where it is known as a virtual state, and eventually becomes a bound state when it passes through the origin into the upper half k plane. The other pole moves down the axis on a trajectory whose ultimate fate depends on the detailed properties of the short-ranged potential. For $l>0$, a virtual state is never formed, as the resonance pole collides with its image pole at $k=0$ and then moves on to become a bound state.

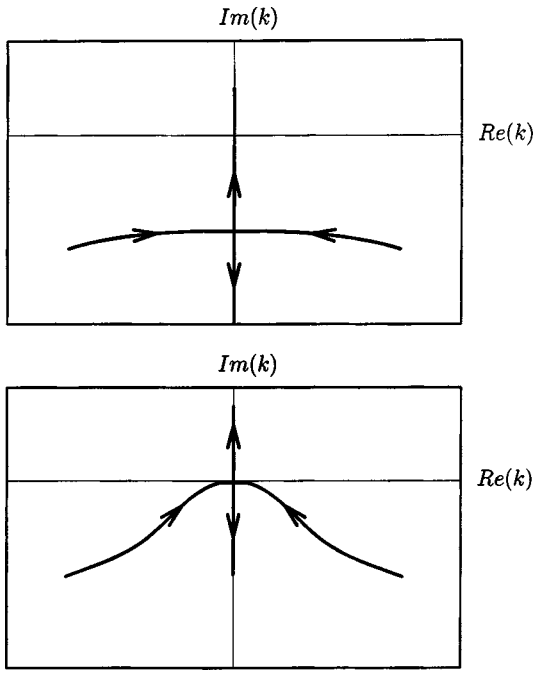

FIG. 1. The trajectories of the poles $S(k)$, as a function of increasing well depth, for the single-channel potential model discussed in text. Upper panel: $l=0$; lower panel: $l=1$.

The situation just described is significantly altered if l is allowed to take on noninteger values. Specifically, we consider the case where

$$V(r)=\begin{cases} -V_0(r), & r<r_0 \\ -\dfrac{d}{r^2}, & r\geqslant r_0, d>0. \end{cases} \tag{5}$$

This potential has been investigated previously as a model for low-energy electron scattering by polar molecules [13–15], since it is related to the radial scattering problem associated with the nodeless angular mode that emerges from a consideration of electron scattering by a fixed point-dipole potential [16]. If the short-range potential in Eq. (5) is a square well, $V_0(r)=-V_0$, the solution can be written in closed form. (The conclusions we will draw here are not limited by our choice of a square-well for the short-range potential. We have considered other choices for $V_0(r)$, such as an exponential or a Gaussian well, which require a purely numerical treatment, and the behavior of $S(k)$ we found was qualitatively unchanged.)

Since the wave function must be regular at $r=0$, $\psi(k,r)$ must be proportional to $\sin(Kr)$ for $r<r_0$, where $K=\sqrt{k^2+2V_0}$. The object we seek is the S matrix, so we write $\psi(k,r)$, for $r\geqslant r_0$, as a linear combination of incoming and outgoing Ricatti-Hankel functions:

$$\psi_L(k,r)=A_1(k)h_L^-(kr)-A_2(k)h_L^+(kr) \tag{6}$$

with the effective angular momentum, L, defined by

$$L(L+1)/2\equiv d. \tag{7}$$

For our purposes here, it will suffice to restrict our attention to values of d less than $\frac{1}{8}$, the so-called critical value [17]; for $0<d<\frac{1}{8}$, L is real. We follow Taylor [18] in defining the Ricatti-Hankel functions as

$$h_L^{+,-}(z)\equiv \pm i\sqrt{\frac{\pi z}{2}}H_\nu^{1,2}(z) \tag{8}$$

with

$$\nu=L+1/2=(\tfrac{1}{4}-2d)^{1/2} \tag{9}$$

so that they have the asymptotic normalization

$$h_L^{+,-}(z)\sim e^{\pm i(z-L\pi/2)}. \tag{10}$$

With these definitions, we see, by comparing Eq. (6) with Eqs. (3) and (10), that $S(k)$ is given by $e^{-iL\pi}A_2(k)/A_1(k)$. By requiring continuity of the logarithmic derivative of the wave function at $r=r_0$, we arrive at an expression for $S(k)$:

$$S(k)=e^{-iL\pi}\frac{kh_L^-(kr_0)'-K\cot(Kr_0)h_L^-(kr_0)}{kh_L^+(kr_0)'-K\cot(Kr_0)h_L^+(kr_0)}=e^{-iL\pi}\frac{[(L+1)-Kr_0\cot(Kr_0)]h_L^-(kr_0)-kr_0h_{L+1}^-(kr_0)}{[(L+1)-Kr_0\cot(Kr_0)]h_L^+(kr_0)-kr_0h_{L+1}^+(kr_0)}. \tag{11}$$

For noninteger L, the Hankel functions $h_L^{+,-}(z)$ are multivalued functions and have a branch point at $z=0$. If L is irrational, then there will be an infinite number of Riemann sheets. The placement of the branch cut is critical to any discussion of the poles of the S matrix. If we wish to establish symmetry relations for $S(k)$ analogous to Eq. (4), then the branch cut must be placed along the negative *imaginary* axis [19]. In previous work [14,20], this was done by using power series expansions of the Bessel functions about the origin.

Unfortunately, the standard definition for Bessel functions with noninteger L [21] places the branch cut along the negative *real* axis, and this is the convention followed in most of the commonly used computer library routines for computing Bessel functions. If one uses routines that follow this standard convention, then one must use analytic continuation to redefine the Hankel functions in the third quadrant so that they are continuous across the negative real axis [measuring positive $\arg(z)$ counterclockwise from the positive real z axis]. With this convention, the *physical sheet* is defined by

$-\frac{1}{2}\pi<\arg(z)<\frac{3}{2}\pi$, with the branch along the negative imaginary axis. The S matrix will have different values on each Riemann sheet; when L is an integer, the discontinuities across the branch cut vanish and $S(k)$ is single-valued.

To establish symmetry relationships between $S(k)$ in the third and fourth quadrants of the physical sheet, we show explicitly how to move the branch cut to the negative imaginary axis. To do this, we start with z in the fourth quadrant and use a variant of the Schwartz reflection principle [21] to obtain:

$$H_\nu^1(z)=H_\nu^2(z^*)^*, \tag{12}$$

which relates the Hankel functions in the fourth quadrant to those in the first quadrant. To complete the exercise, we need to further rotate z by π to move it into the third quadrant. This can be done by using the so-called circuit relations for the Hankel functions [21,22]:

$$\sin(\nu\pi)H_\nu^1(ze^{im\pi})=-\sin[(m-1)\nu\pi]H_\nu^1(z) - e^{i\nu\pi}\sin(m\nu\pi)H_\nu^2(z), \tag{13}$$

$$\sin(\nu\pi)H_\nu^2(ze^{im\pi})=\sin[(m+1)\nu\pi]H_\nu^2(z) + e^{i\nu\pi}\sin(m\nu\pi)H_\nu^1(z). \tag{14}$$

Combining Eqs. (12) and (13) with $m=1$, and using the definition in Eq. (8), we can easily derive the relation:

$$h_L^+(e^{i\pi}z^*)=e^{-iL\pi}h_L^+(z)^*, \tag{15}$$

which properly defines h_L^+ in the third (or second) quadrant of the physical sheet in terms of $h_L^+(z)$ in the fourth (or first) quadrant. Equation (15), along with Eq. (11), are sufficient to establish that the poles of $S(k)$, on the physical sheet, are located symmetrically with respect to the imaginary k axis.

The symmetry relation for $h_L^-(kr)$ analagous to Eq. (15) is a bit more involved. By using Eq. (14), again with $m=1$, and Eq. (12), we can derive, after some algebra, the relation

$$h_L^-(e^{i\pi}z^*)=e^{iL\pi}h_L^-(z)^*-2i\sin(L\pi)h_L^+(z)^*. \tag{16}$$

Equations (15) and (16) can be used to derive the following remarkable symmetry relation for $S(k)$ on the physical sheet:

$$S(k)+e^{iL\pi}=S(-k^*)^*+e^{-iL\pi} \tag{17}$$

which reduces to the more familiar Eq. (4) when L is an integer.

We can also derive symmetry relations for $S(k)$ on other Riemann sheets. These are reached from the physical sheet, following the labeling conventions of Herzenberg [14], by rotating z through the branch cut in either a clockwise $[\arg(z)<-\pi/2]$ or counterclockwise $[\arg(z)>3\pi/2]$ direction. By using the circuit relations with even values of m, it is possible to show that Eqs. (15) and (16) establish a general relationship between the Hankel functions evaluated in the right-half planes of the *clockwise* Riemann sheets and the left-half planes of the corresponding *counterclockwise* Riemann sheets. Thus, the symmetry relation for $S(k)$ expressed in Eq. (17) is similarly mirrored between the higher clockwise and counterclockwise Riemann sheets.

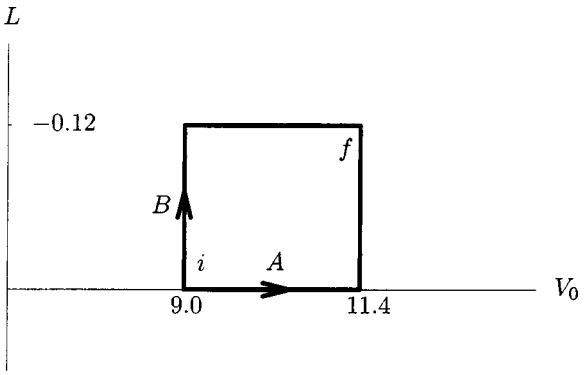

FIG. 2. The parameters of the one-channel model discussed in text, namely the depth of the square well, V_0, and the effective L value, are changed along two different paths. Both paths start at i and end at f. On path A, the depth of the square well is first increased and then L is decreased. On path B, the order is reversed. All quantities are in atomic units.

We are now in a position to discuss the trajectories of the poles of $S(k)$ for this model problem. In particular, we want to see how the presence of a weak r^{-2} potential tail causes the pole trajectories to change from the behavior typically expected with short-ranged potentials. This line of analysis has been given previously [14,15,19], but it is important to review it here before going on to a multichannel generalization of this model. We start with the radial square well with a range, r_0, of 1 Bohr and a depth, V_0, of 9.0 Hartree and an infinitesimally small (but finite) dipole tail, i.e., $L\approx 0$. With this choice, there are a pair of complex poles near $k=\pm 1-i1.75$ on all Riemann sheets. If the well depth is increased to 11.4 Hartree and L is decreased to -0.12, the potential will support a single, weakly bound state. Now consider two different paths for reaching the final state, which are depicted in Fig. 2. First, we increase the potential well from 9.0 to 11.4 Hartree with $L\approx 0$ and then decrease L to -0.12. We designate this as path A. Alternatively, we can first decrease L from 0 to its final value and then deepen the potential well. We designate this as path B.

Figure 3 shows the pole trajectories, for paths A and B, on both the physical sheet and the first Riemann sheet. For ease of visualization, we only plot the trajectories on the right half of the physical sheet and the left half of the first clockwise sheet in Fig. 3; the mirror image trajectories on the left half of the physical sheet and the right half of the first counterclockwise sheet are not shown. Along the first portion of path A, the poles move from their initial positions toward the negative imaginary axis on trajectories that are virtually identical on both sheets. However, since L is infinitesimal but finite, the trajectories do not quite hit the axis. Moreover, we can see clearly that it is the trajectories on the second sheet that move up along the negative imaginary axis toward the origin, while those on the physical sheet travel downward. When L is then decreased, the poles on the physical sheet move further away from the negative imaginary axis while those on the unphysical sheets follow quasi-parabolic paths

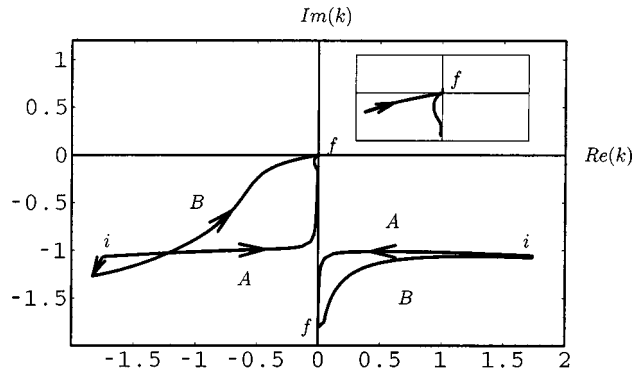

FIG. 3. Trajectories of the *S*-matrix poles in the complex momentum plane for the potential scattering problem discussed in text. The depth of the square-well and the strength of the r^{-2} tail are varied according to the paths designated in Fig. 2. Note that the curve on the right is on the physical sheet, while that on the left is on the first clockwise (unphysical) sheet. The mirror trajectories on the physical and first counterclockwise sheets are not shown for ease of visualization. The inset shows the behavior near the origin in finer detail. All quantities are in atomic units.

into the origin to form the bound state. If we now track the resonances on path B, the poles reach the same final positions on paths that do not parallel the imaginary axis. From these plots, it is clear that it is not the poles on the physical sheet that become bound states as the potential is strengthed, but rather those arriving at the origin from the unphysical sheets.

It is only the poles that lie in the fourth quadrant of the physical sheet that can have any visible effect on the cross sections and hence the poles on unphysical sheets can have no observable features until they emerge as bound states. It is a property of potentials with an attractive r^{-2} tail that resonance poles do not ''connect'' to bound states. It should also be mentioned that for potentials with a *repulsive* r^{-2} tail, bound states do not necessarily disappear through the cut as the potential is weakened and can stay on the physical sheet as they move into the lower-half *k* plane.

III. A SOLVABLE TWO-CHANNEL MODEL

Low-energy electron-CO_2 scattering is characterized by two prominent features: a virtual state enhancement of the cross section at very low energies and a shape resonance near 4 eV. *Ab initio* studies carried out in linear geometry have confirmed that these features are associated with the $^2\Sigma_g^+$ and $^2\Pi_u$ components of the wave function, respectively. In linear geometry, these features are not coupled and can be studied independently. When the target molecule is bent, the virtual and resonance states are affected by additional features associated with the symmetry breaking. In particular, bending induces a dipole moment in the target. To study these effects, we employ a simple two-channel extension of the previous model. We look at a two-channel potential scattering problem with degenerate energy thresholds that includes only *s* and *p* waves, which are the leading terms in a single-center expansion of the $^2\Sigma_g^+$ and $^2\Pi_u$ components of the scattering wave function; the two channels are coupled by a dipole interaction. The coupled-channel Schrödinger equation we consider is

$$\begin{pmatrix} -\frac{1}{2}\frac{d^2}{dr^2}+V_0(r)-k^2/2 & C(r) \\ C(r) & -\frac{1}{2}\frac{d^2}{dr^2}+V_1(r)-k^2/2 \end{pmatrix} \times \begin{pmatrix} \psi_0(r) \\ \psi_1(r) \end{pmatrix} = 0, \tag{18}$$

where

$$C(r) \underset{r\to\infty}{\sim} d/r^2 \tag{19}$$

and

$$V_1(r) \underset{r\to\infty}{\sim} 1/r^2. \tag{20}$$

For a particular choice of potentials, we can again get an analytic solution. To this end, we define:

$$V_0(r) = \begin{cases} -V_0, & r<r_0 \\ 0, & r\geqslant r_0, \end{cases} \tag{21}$$

$$V_1(r) = \begin{cases} -V_1, & r<r_0 \\ \dfrac{1}{r^2}, & r\geqslant r_0, \end{cases} \tag{22}$$

$$C(r) = \begin{cases} 0, & r<r_0 \\ \dfrac{d}{r^2}, & r\geqslant r_0. \end{cases} \tag{23}$$

For $r<r_0$, we have two uncoupled square wells, so the two linearly independent solution vectors are

$$\Psi \propto \begin{pmatrix} \sin(K_0 r) & 0 \\ 0 & \sin(K_1 r) \end{pmatrix} \equiv \mathbf{\Psi_0}, \quad r<r_0 \tag{24}$$

with $K_{(0,1)}=\sqrt{k^2+2V_{(0,1)}}$. For $r\geqslant r_0$, the potential matrix is

$$\mathbf{V} = (1/r^2)\begin{pmatrix} 0 & d \\ d & 1 \end{pmatrix} \equiv (1/r^2)\mathbf{D}, \quad r\geqslant r_0. \tag{25}$$

Let **U** be the unitary matrix that diagonalizes **D**:

$$\mathbf{U^{-1}DU} = \begin{pmatrix} \lambda_0 & 0 \\ 0 & \lambda_1 \end{pmatrix}. \tag{26}$$

The eigenvalues are given by

$$\lambda_0=\frac{1-(1+4d^2)^{1/2}}{2}\equiv L_0(L_0+1)/2,$$

$$\lambda_1=\frac{1+(1+4d^2)^{1/2}}{2}\equiv L_1(L_1+1)/2. \quad (27)$$

We can therefore express the wave function beyond r_0 as

$$\Psi\propto\mathbf{U}\left[\begin{pmatrix} h^-_{L_0}(kr) & 0 \\ 0 & h^-_{L_1}(kr)\end{pmatrix} - \begin{pmatrix} h^+_{L_0}(kr) & 0 \\ 0 & h^+_{L_1}(kr)\end{pmatrix}\mathbf{S^L}\right]$$

$$\equiv\mathbf{U}[\mathbf{h^-_L}(\mathbf{r})-\mathbf{h^+_L}(\mathbf{r})\mathbf{S^L}],\quad r\geqslant r_0, \quad (28)$$

where $\mathbf{S^L}$ is the S matrix in the ''dipole'' basis. By requiring continuity of the logarithmic derivative of Ψ at r_0, we get an expression for $\mathbf{S^L}$:

$$\mathbf{S^L}=\left[\frac{d}{dr}\mathbf{h^+_L}(\mathbf{r_0})-\mathbf{U^{-1}}\left(\frac{d}{dr}\mathbf{\Psi_0}\right)\mathbf{\Psi_0^{-1}}\mathbf{U}\mathbf{h^+_L}(\mathbf{r_0})\right]^{-1}$$

$$\times\left[\frac{d}{dr}\mathbf{h^-_L}(\mathbf{r_0})-\mathbf{U^{-1}}\left(\frac{d}{dr}\mathbf{\Psi_0}\right)\mathbf{\Psi_0^{-1}}\mathbf{U}\mathbf{h^-_L}(\mathbf{r_0})\right]. \quad (29)$$

Finally, to obtain the physical S matrix, $\mathbf{S^0}$, in terms of $\mathbf{S^L}$, we compute

$$\mathbf{S^0}=\mathbf{e^{il\pi/2}}\mathbf{U}\mathbf{e^{iL\pi/2}}\mathbf{S^L}\mathbf{e^{iL\pi/2}}\mathbf{U^{-1}}\mathbf{e^{il\pi/2}}, \quad (30)$$

where, in an obvious notation, $\mathbf{e^{iL\pi/2}}$ and $\mathbf{e^{il\pi/2}}$ are diagonal matrices with eigenvalues $(e^{iL_0\pi/2},e^{iL_1\pi/2})$ and $(1,i)$, respectively. We see from Eq. (29) that the poles of the S matrix are given by the condition:

$$\det\left[\frac{d}{dr}\mathbf{h^+_L}(\mathbf{r_0})-\mathbf{U^{-1}}\left(\frac{d}{dr}\mathbf{\Psi_0}\right)\mathbf{\Psi_0^{-1}}\mathbf{U}\mathbf{h^+_L}(\mathbf{r_0})\right]=0. \quad (31)$$

The model can obviously be extended to include any number of channels and is the generalization of the one-channel model considered in the previous section. The key element which makes for an analytically solvable model is the truncation of both the diagonal centrifugal terms and the coupling terms in the interior region.

With this two-channel model, we can study a problem that mimics the essential features found in the case of CO_2: we choose the potential parameters so that, in the absence of any channel-coupling, the potential V_0 will support a virtual state and V_1 will show a resonance. These features can be tuned independently by varying the two well depths. Since bending couples s and p waves and produces an electron-dipole interaction, it can be modeled by varying the strength of the off-diagonal coupling. Stretching, on the other hand, could be modeled by changing the two well depths. In principle, we have three parameters that can be independently varied. In our previous *ab initio* calculations [7] we found a strong dependence of the shape resonance on symmetric stretch motion and less so in the case of the virtual state. We will therefore limit ourselves to an independent investigation of only two parameters, the well depth V_1 in the p-wave channel and the channel coupling d.

IV. TWO-CHANNEL MODEL WITH SHORT-RANGE COUPLING

It is instructive to first look at a case where there is only short-range coupling to get a basic picture of what can happen and then see how that picture is modified in the presence of dipole coupling. If we replace the coupling term in Eq. (23) with

$$C(r)=\begin{cases} d, & r<r_0 \\ 0, & r\geqslant r_0\end{cases} \quad (32)$$

we can again solve the problem analytically along the lines outlined in the previous section.

A moment's reflection makes it clear what to expect. If the well depth V_1 is increased, in the presence of a very weak coupling, then the resonance will move toward the origin on its path to becoming a bound state. However, because of the finite coupling to the s-wave channel, the resonance can always escape through the s-wave channel even at the point at which it is about to become a bound state. Thus the point at which the resonance collides with its image from the lower left quadrant to form a double pole will lie on the negative imaginary k axis, just *below* the origin, i.e., the resonance approaches the origin as a virtual state. The weak coupling will also have an effect on the virtual state in the s-wave channel. It moves a bit closer to the origin, reflecting the fact that it can detour, because of the coupling, to the p-wave channel before leaking to the s-wave continuum. As the well depth V_1 is further increased, the initial resonance goes on to become a bound state while its image moves down the imaginary axis, eventually colliding with the quasi-stationary initial virtual state. The latter two then split and move away from the axis in the lower half plane. This case is depicted in the top panel of Fig. 4.

If the coupling is increased, then the effects described above become more pronounced: the point at which the resonance collides with its image moves further down the imaginary axis and the virtual state moves further up. For some critical value of the initial coupling, the point at which the resonance collides with its image as the well is deepened can be made to coincide with the point at which they both touch the trajectory of the initial virtual state: i.e., a triple pole can be formed. Because of the symmetry that must exist between the left- and right-half planes, the triple pole must, of necessity, lie on the imaginary axis. This case is depicted in the center panel of Fig. 4.

Finally, for coupling strengths greater than this critical value, it is the initial virtual state that moves up the origin to become bound, while the resonance and its image pole are turned away before they reach the imaginary axis and move off into the lower half of the complex k plane. That case is depicted in the bottom panel of Fig. 4.

But there is now seemingly a paradox. For the case depicted in Fig. 4(bottom), it is the virtual state that becomes a bound state. It will remain bound if, from the final state, we then reduce the coupling to the value used in Fig. 4(top). Conversely, for the case depicted in Fig. 4(top), it is the resonance state that becomes bound; it will remain bound if,

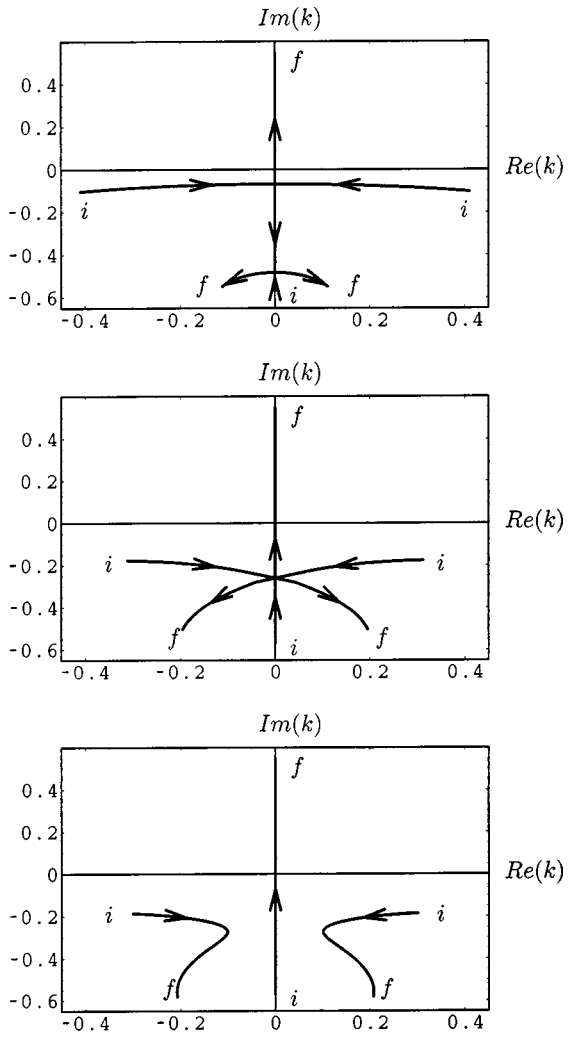

FIG. 4. *S*-matrix pole trajectories in the complex momentum plane for a two-channel square well with short-range coupling. The well depth V_0 is fixed at 0.75 bohr and the well depth, V_1, is increased from an initial value (*i*) of 1.8 bohr, in which there is no bound state, to a final value (*f*) of 2.4 bohr, which produces a bound state. The three panels correspond, from top to bottom, to increased coupling between the channels. The center panel shows the trajectory for a value of coupling parameter that produces an exact degeneneracy of the resonance and virtual states. All quantities are in atomic units.

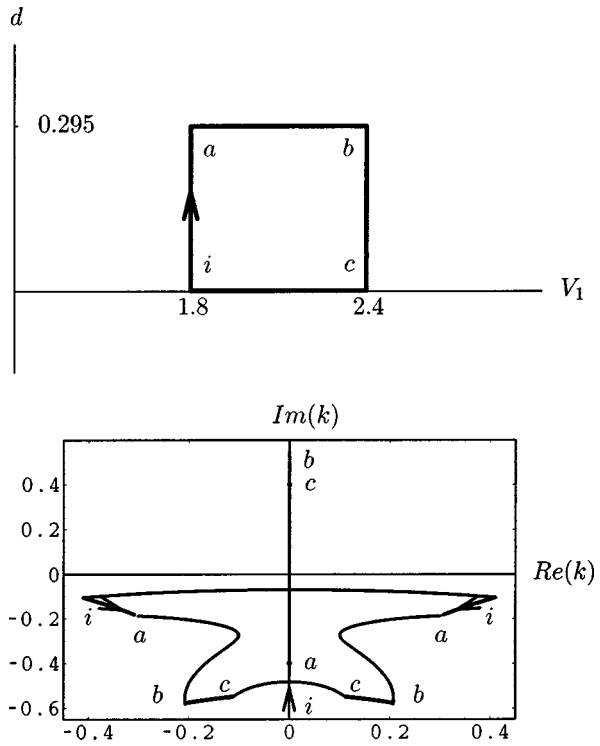

FIG. 5. Two-channel square well with short-range coupling. Trajectories of the *S*-matrix poles in the complex *k* plane when the well depth, V_1, and coupling strength, *d*, are varied around the closed loop shown in the top panel. V_1 is varied between 1.8 and 2.4 and *d* is varied between 0.0 and 0.295. The well depth V_0 is fixed at 0.75. All quantities are in atomic units.

from the final state, the coupling is then increased to the value used in the bottom panel. It appears that the final state somehow depends on the path used to reach it, i.e., it is not uniquely determined by the potential parameters.

To make this picture clearer, we can, as we did in the one channel case, plot the trajectories of the initial resonance and virtual states along a closed path. The trajectories are plotted in Fig. 5. Along the first segment of the path (from *i* to *a*), the virtual state moves slightly up the imaginary axis, while the resonance and its image pole begin to approach each other in the lower half *k* plane. From *a* to *b*, where the well depth is increased, the virtual state moves up the imaginary axis to become bound, while the resonance and its image are first attracted and then turned away from each other in the lower half plane. As the coupling strength is reduced from *b* to *c*, the bound state moves slightly closer to the origin, while the resonance and its image pole again move toward each other. Finally, from *c* to *i*, where the well depth is reduced to its initial value, the bound state further descends while the resonance and its image collide on the negative imaginary axis; one pole then moves down to the position originally occupied by the virtual state, while the other moves up the axis. It collides with the decending pole just below the origin and the two poles move away from the imaginary axis to the positions originally occupied by the resonance poles. Thus after one loop around the closed path, the resonance and virtual states have exchanged places.

The associated wave functions must therefore differ only by a phase factor from those of the corresponding initial states. It takes two complete loops around the closed path before both poles return to their initial positions. We also note that the particular values of well depth and coupling which produce the triple degeneracy discussed above must lie inside the closed loop we have constructed that produces the trajectories shown in Fig. 5. The implication, of course, is that the point of triple degeneracy, shown in Fig. 4(center), corresponds to a conical intersection on the resonance surface and that there is a Berry phase associated with any closed path that encircles this point. This will be further discussed below.

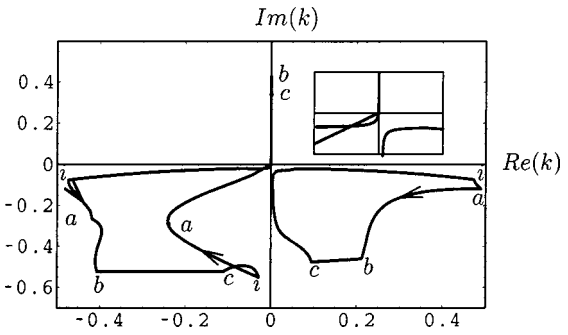

FIG. 6. Two-channel square well with dipole coupling. Trajectories of the *S*-matrix poles in the complex *k* plane when the well depth, V_1, and the coupling strength, *d*, are varied around a closed loop of the type shown in Fig. 5. The well depth V_0 is fixed at 0.75 and V_1 is varied between 1.8 and 2.4. The coupling parameter is varied between 0.05 and 0.195. The curve on the right is on the physical sheet, while that on the left is on the first clockwise (unphysical) sheet. There are mirror trajectories in the lower left physical and lower right first counterclockwise sheets, respectively, which are not shown for ease of visualization. The inset shows the behavior near the origin in finer detail. All quantities are in atomic units.

V. TWO-CHANNEL MODEL WITH DIPOLE COUPLING

With long-range dipole coupling between the channels, the *S* matrix is again a multivalued function in the plane of complex momentum. Equation (31) shows that, just as in the single-channel case, the poles of the *S* matrix, because of the properties of $h_L^+(z)$, will be found in symmetric pairs on different Riemann sheets. It is significant that the effective angular momenta, L_0 and L_1, determined from the eigenvalues given by Eq. (27), are independent of the sign of the coupling strength *d*. In particular, L_0 will *decrease* from zero as the dipole coupling is first turned on. This, in turn, dictates that a bound state will move off the physical sheet as the well depth is decreased in the presence of a finite dipole coupling. With the insight gained from looking at the effects of a potential with an attractive r^{-2} tail in the single-channel case, as well as the two-channel case with short-range coupling just considered, we can finally approach the dipole-coupled two-channel problem.

Once again, we study a case where, in the absence of any coupling, the initial potential well depths are chosen to produce a resonance and a virtual state. We then choose a very small, but finite, value for the initial coupling so that we can unambiguously track the identity of the poles on the various Riemann sheets. Figure 6 shows the pole trajectories that are produced as the potential parameters V_1 and *d* are varied around a closed loop of the kind used to produce Fig. 5 in the case of short-range coupling. On the physical sheet, the resonance pole and its image (not shown) trace closed paths in the lower-half *k* plane after a single loop in the two-parameter (V_1,d) space. Bound states are never formed. On the unphysical sheets, we get a different picture. The trajectory in the third quadrant of the first clockwise sheet (and its image in the right counterclockwise sheet) shows the same kind of behavior we saw in the two-channel, short-range example: in one complete cycle, the resonance, after evolving to become a bound state along part of its trajectory, goes on to exchange places with the initial virtual state which lay originally not on the negative imaginary axis, but just off it. It takes another full cycle to get both poles back to their original positions. This implies that there is again a conical intersection that the trajectories have encircled, but with dipole channel-coupling, the conical intersection is now a double pole of the *S* matrix on the unphysical Riemann sheets and corresponds to a degeneracy of the virtual state and the resonance.

VI. BERRY PHASE

Since the appearance of Berry's [23] much celebrated article, there have been many papers dealing with the geometric phases accumulated by the wave functions for systems that are adiabatically transported about a closed circuit in some physical parameter space. Much of this literature has focused on phenomena connected with accidentally degenerate eigenvalues in systems described by Hermitian Hamiltonians, but more recently, several authors have shown that degeneracies are possible in the case of resonance states that have complex energies. Pont *et al.* [24], for example, have studied geometric phases in multiphoton ionization, illustrating how the autoionizing states of an atom in a bichromatic field circumnavigate a degeneracy when physical parameters of the laser field are varied. Kylstra and Joachain [25] have published a related study of the double poles of the *S* matrix that can occur in laser-assisted electron-atom collisions while Vanroose [26] has investigated inducing degeneracy between two resonant states in a double well structure.

In the present case, we are considering a Hamiltonian that depends on two real parameters, ν and λ, which are being varied. We assume that for a particular choice (ν_0,λ_0), there are two resonant scattering states, ψ_a and ψ_b with complex energies E_a and E_b that satisfy

$$[H(\nu_0,\lambda_0)-E_a]\psi_a=0,$$

$$[H(\nu_0,\lambda_0)-E_b]\psi_b=0. \tag{33}$$

The resonance states are assumed to be normalized by a suitable analytic continuation procedure, such as regularization or contour integration [27] and the orthogonality relation between the two states is defined without complex conjugation:

$$\int \psi_a\psi_b=0. \tag{34}$$

For small changes in the parameters about ν_0 and λ_0, we can write the Hamiltonian as

$$H(\nu,\lambda)=H(\nu_0,\lambda_0)+\left.\frac{\partial H}{\partial \nu}\right|_{\nu_0}\delta\nu+\left.\frac{\partial H}{\partial \lambda}\right|_{\lambda_0}\delta\lambda\equiv H_0+H'. \tag{35}$$

If we further assume that the resonance states are close to being degenerate, then in the vicinity of the degeneracy, a

solution $\psi(\nu,\lambda)$ corresponding to the altered Hamiltonian can be written as a linear combination of ψ_a and ψ_b,

$$\psi(\nu,\lambda)=A(\nu,\lambda)\psi_a+B(\nu,\lambda)\psi_b, \tag{36}$$

and the equation for $\psi(\nu,\lambda)$ now becomes a 2×2 complex symmetric matrix equation that determines the coefficients A and B:

$$\begin{pmatrix} E_a-E+\langle\psi_a|H'|\psi_a\rangle & \langle\psi_a|H'|\psi_b\rangle \\ \langle\psi_a|H'|\psi_b\rangle & E_b-E+\langle\psi_b|H'|\psi_b\rangle \end{pmatrix} \times\begin{pmatrix} A \\ B \end{pmatrix}=0. \tag{37}$$

If we shift the energy scale to measure E from the centroid of the diagonal terms,

$$E\rightarrow E-\frac{E_a+\langle\psi_a|H'|\psi_a\rangle+E_b+\langle\psi_b|H'|\psi_a\rangle+E_b}{2}, \tag{38}$$

then the 2×2 matrix in Eq. (37) can be rewritten as

$$Z(\nu,\lambda)\sigma_z+X(\nu,\lambda)\sigma_x-E\mathbf{I}, \tag{39}$$

with

$$\sigma_x=\begin{pmatrix} 0 & 1 \\ 1 & 0 \end{pmatrix} \quad \text{and} \quad \sigma_z=\begin{pmatrix} -1 & 0 \\ 0 & 1 \end{pmatrix}, \tag{40}$$

and the eigenvalues are therefore given by

$$E^{\pm}=\pm\sqrt{Z^2+X^2}. \tag{41}$$

The eigenvalues are degenerate when either

$$Z(\nu,\lambda)+iX(\nu,\lambda)=0 \tag{42}$$

or

$$Z(\nu,\lambda)-iX(\nu,\lambda)=0. \tag{43}$$

Since Z and X are complex numbers, the real and imaginary parts of Eqs. (42) or (43) must both be satisfied, which means both ν and λ must be varied to produce a degeneracy. In contrast, for bound states described by a Hermitian Hamiltonian, it is generally necessary to vary three parameters to make a degeneracy occur accidentally.

Suppose $H(\nu,\lambda)$ has a degeneracy for the parameters ν_d and λ_d and we vary ν and λ in a loop around these values such that

$$Z^2(\nu,\lambda)+X^2(\nu,\lambda)=\rho^2, \tag{44}$$

where ρ is a constant complex number. We can then express Z and X in terms of a real angle θ as

$$Z(\nu,\lambda)=\rho\cos\theta, \tag{45}$$

$$X(\nu,\lambda)=\rho\sin\theta. \tag{46}$$

From Eq. (41), the two eigenvalues are now $E^{\pm}=\pm\rho$ and the coefficients $A^{\pm}$ and $B^{\pm}$ that satisfy Eq. (37) fit the equation

$$\begin{pmatrix} \rho\cos\theta-(+)\rho & \rho\sin\theta \\ \rho\sin\theta & -\rho\sin\theta-(+)\rho \end{pmatrix}\begin{pmatrix} A^{\pm}(\theta) \\ B^{\pm}(\theta) \end{pmatrix}=0. \tag{47}$$

The normalized solutions of Eq. (47) are

$$\begin{pmatrix} A^{+}(\theta) \\ B^{+}(\theta) \end{pmatrix}=\begin{pmatrix} \cos(\theta/2) \\ \sin(\theta/2) \end{pmatrix},$$

$$\begin{pmatrix} A^{+}(\theta) \\ B^{+}(\theta) \end{pmatrix}=\begin{pmatrix} -\sin(\theta/2) \\ \cos(\theta/2) \end{pmatrix}. \tag{48}$$

Thus, after one complete loop in parameter space $\theta\in[0,2\pi]$, the eigenstates undergo a change in sign. Another loop, $\theta\in[2\pi,4\pi]$, is necessary to arrive back in the original position. This is precisely the behavior followed by the virtual and resonance state trajectories discussed in the previous section.

VII. DISCUSSION

We have attempted here to gain further insight into electron-CO_2 collision dynamics with simple models that incorporate key aspects of the physical problem. A two-channel model with *s*- and *p*-wave square wells enables us to study how virtual states and shape resonances interact under the influence of a long-range r^{-2} interaction that mimics the effects of bending in the physical system. The picture that emerges is that a bound state, which evolves smoothly to become a resonance in the linearly constrained system, behaves in a qualitatively different fashion when the target is bent. The dipole field changes the analytic structure of the *S* matrix, making it a multivalued function. Bound-states, however, do not simply vanish in the presence of a dipolar field as the binding potentials are weakened, as was suggested in the early work of Domcke and Cederbaum [28]. They are instead forced onto an unphysical Riemann sheet. This picture is entirely consistent with the behavior of the virtual state observed by Morgan (see Fig. 2 of Ref. [1]) and also explains the resonance behavior observed by Rescigno *et al.* [7]. Our model also shows that ''resonance'' and ''virtual'' states can undergo an accidental degeneracy and form a conical intersection. For short-range coupling, this degeneracy would occur on the negative imaginary *k* axis, but with dipole coupling, it occurs on higher Riemann sheets. We believe that our model provides an explanation of how the resonance and virtual states in the electron-CO_2 system may be connected.

Resonances are ubiquitous in low-energy electron collisions with polyatomic molecules and can provide efficient pathways for channeling electronic energy into nuclear degrees of freedom. It is therefore important to understand how the topology of molecular negative ion resonance surfaces can impact processes such as resonant vibrational excitation or dissociative electron attachment. We hope that this study will lead to further work in this area.

ACKNOWLEDGMENTS

This work was performed under the auspices of the U.S. Department of Energy by the University of California Lawrence Berkeley National Laboratory and Lawrence Livermore National Laboratory under Contract Nos. DE-AC03-76F00098 and W-7405-Eng-48, respectively. The work was supported by the U.S. DOE Office of Basic Energy Science, Division of Chemical Sciences.

[1] L.A. Morgan, Phys. Rev. Lett. **80**, 1873 (1998).
[2] M.A. Morrison, Phys. Rev. A **25**, 1445 (1982).
[3] T.N. Rescigno, D.A. Byrum, W.A. Isaacs, and C.W. McCurdy, Phys. Rev. A **60**, 2186 (1999).
[4] C.-H. Lee, C. Winstead, and V. McKoy, J. Chem. Phys. **111**, 5056 (1999).
[5] D. Field, N.C. Jones, S.L. Lunt, and J.-P. Ziesel, Phys. Rev. A **64**, 022708 (2001).
[6] M. Allan, Phys. Rev. Lett. **87**, 033201 (2001).
[7] T.N. Rescigno, W.A. Isaacs, A.E. Orel, H.-D. Meyer, and C.W. McCurdy, Phys. Rev. A **65**, 032716 (2002).
[8] D.G. Hopper, Chem. Phys. **53**, 85 (1980).
[9] G.L. Gutsev, R.J. Bartlett, and R.N. Compton, J. Chem. Phys. **108**, 6756 (1998).
[10] B.L. Whitten and N.F. Lane, Phys. Rev. A **26**, 3170 (1982).
[11] H. Estrada and W. Domcke, J. Phys. B **18**, 4469 (1985).
[12] S. Mazevet, M.A. Morrison, L.A. Morgan, and R.K. Nesbet, Phys. Rev. A **64**, 040701(R) (2001).
[13] A. Herzenberg and B.C. Saha, J. Phys. B **16**, 591 (1983).
[14] A. Herzenberg, J. Phys. B **17**, 4213 (1984).
[15] H. Estrada and W. Domcke, J. Phys. B **17**, 279 (1984).
[16] M.H. Mittleman and R.E. von Holdt, Phys. Rev. **140**, A726 (1965).
[17] O.H. Crawford, Proc. Phys. Soc. London **91**, 279 (1967).
[18] J.R. Taylor, *Scattering Theory: The Quantum Theory on Nonrelativistic Collisions* (Wiley, New York, 1972).
[19] R.G. Newton, *Scattering Theory of Particles and Waves*, 2nd ed. (Springer-Verlag, New York, 1982).
[20] R. Fandreyer and P.G. Burke, J. Phys. B **29**, 339 (1996).
[21] *Handbook of Mathematical Functions*, edited by M. Abramowitz and I.A. Stegun (National Bureau of Standards, Washington, D.C., 1964).
[22] *Higher Transcendental Functions*, edited by A. Erdelyi (McGraw-Hill, New York, 1953).
[23] M.V. Berry, Proc. R. Soc. London, Ser. A **392**, 45 (1984).
[24] R.S.M. Pont, P.M. Potvliege, and P.H.G. Smith, Phys. Rev. A **46**, 555 (1992).
[25] N.J. Kylstra and C.J. Joachain, Phys. Rev. A **57**, 412 (1998).
[26] W. Vanroose, Phys. Rev. A **64**, 062708 (2001).
[27] T.N. Rescigno and C.W. McCurdy, Phys. Rev. A **34**, 1882 (1986).
[28] W. Domcke and L.S. Cederbaum, J. Phys. B **14**, 149 (1980).